Porous fibers: a novel approach to low loss THz waveguides

Shaghik Atakaramians[1,2], Shahraam Afshar V.[1], Bernd M. Fischer[2], Derek Abbott[2] and Tanya M. Monro[1]

[1]*Centre of Expertise in Photonics, School of Chemistry & Physics,*
[2]*Centre for Biomedical Engineering, School of Electrical & Electronic Engineering,*
The University of Adelaide, SA 5005 Australia
shaghik@eleceng.adelaide.edu.au

Abstract: We propose a novel class of optical fiber with a porous transverse cross-section that is created by arranging sub-wavelength air-holes within the core of the fiber. These fibers can offer a combination of low transmission loss and high mode confinement in the THz regime by exploiting the enhancement of the guided mode field that occurs within these sub-wavelength holes. We evaluate the properties of these porous fibers and quantitatively compare their performance relative to that of a solid core air cladded fiber (microwire). For similar loss values, porous fibers enable improved light confinement and reduced distortion of a broadband pulse compared to microwires.

OCIS codes: (230.7370) Waveguides; (130.2790) Guided waves; (260.3090) Infrared, far.

References and links

1. D. Abbott and X.-C. Zhang, "Scanning the issue: T-ray imaging, sensing, and retection," Proceedings of the IEEE **95**, 1509–1513 (2007).
2. K. Sakai, *Terahertz Optoelectronics* (Springer, Berlin, and Heidlberg, 2005).
3. W. Withayachumnankul, G. M. Png, X. Yin, S. Atakaramians, I. Jones, H. Lin, B. Ung, J. Balakrishnan, B. W.-H. Ng, B. Ferguson, S. P. Mickan, B. M. Fischer, and D. Abbott, "T-ray sensing and imaging," Proceedings of the IEEE **95**, 1528–1558 (2007).
4. B. M. Fischer, M. Hoffmann, H. Helm, R. Wilk, F. Rutz, T. Kleine-Ostmann, M. Koch, and P. U. Jepsen, "Terahertz time-domain spectroscopy and imaging of artificial RNA," Opt. Express **13**, 5205–5215 (2005).
5. R. W. McGowan, G. Gallot, and D. Grischkowsky, "Propagation of ultrawideband short pulses of terahertz radiation through submillimeter-diameter circular waveguides," Opt. Express **24**(20), 1431–1433 (1999).
6. G. Gallot, S. P. Jamison, R. W. McGowan, and D. Grischkowsky, "Terahertz waveguides," J. Opt. Soc. Am. B **17**, 851–863 (2000).
7. S. P. Jamison, R. W. McGowan, and D. Grischkowsky, "Single-mode waveguide propagation and reshaping of sub-ps terahertz pulses in sapphire fibers," Appl. Phys. Lett. **76**, 1987–1989 (2000).
8. R. Mendis and D. Grischkowsky, "Plastic ribbon THz waveguides," J. Appl. Phys. **88**, 4449–4451 (2000).
9. R. Mendis and D. Grischkowsky, "Undistorted guided-wave propagation of subpicosecond terahertz pulses," Opt. Lett. **26**, 846–848 (2001).
10. R. Mendis and D. Grischkowsky, "THz interconnect with low-loss and low-group velocity dispersion," Microwave and Wireless Components Letters **11**, 444–446 (2001).
11. H. Han, H. Park, M. Cho, and J. Kim, "Terahertz pulse propagation in a plastic photonic crystal fiber," Appl. Phys. Lett. **80**, 2634–2636 (2002).
12. T.-I. Jeon and D. Grischkowsky, "Direct optoelectronic generation and detection of sub-ps-electrical pulses on sub-mm-coaxial transmission lines," Appl. Phys. Lett. **85**, 6092–6094 (2004).
13. K. Wang and D. M. Mittleman, "Metal wires for terahertz wave guiding," Nature **432**, 376–379 (2004).
14. T.-I. Jeon, J. Zhang, and K. W. Goossen, "THz Sommerfeld wave propagation on a single metal wire," Appl. Phys. Lett. **86**, 161904 (2005).

15. A. Bingham, Y. Zhao, and D. Grischkowsky, "THz parallel plate photonic waveguides," Appl. Phys. Lett. **87**, 051101 (2005).
16. T.-I. Jeon and D. Grischkowsky, "THz Zenneck surface wave (THz surface plasmon) propagation on a metal sheet," Appl. Phys. Lett. **88**, 061113 (2006).
17. L.-J. Chen, H.-W. Chen, T.-F. Kao, J.-Y. Lu, and C.-K. Sun, "Low-loss subwavelength plastic fiber for terahertz waveguiding," Opt. Lett. **31**(3), 308–310 (2006).
18. R. Mendis, "Nature of subpicosecond terahertz pulse propagation in practical dielectric-filled parallel-plate waveguides," Opt. Lett. **31**(17), 2643–2645 (2006).
19. M. Nagel, A. Marchewka, and H. Kurz, "Low-index discontinuity terahertz waveguides," Opt. Express **14**, 9944–9954 (2006).
20. M. Wächter, M. Nagel, and H. Kurz, "Metallic slit waveguide for dispersion-free low-loss terahertz signal transmission," Appl. Phys. Lett. **90**, 061111 (2007).
21. S. Afshar Vahid, S. Atakaramians, B. M. Fischer, H. Ebendorff-Heidepriem, T. M. Monro, and D. Abbott, "Low loss, low dispersion T-ray transmission in microwires," in *CLEO/QELS*, art. no. JWA105 (Baltimore, Maryland, 2007).
22. J.-Y. Lu, C.-P. Yu, H.-C. Chang, H.-W. Chen, Y.-T. Li, C.-L. Pan, and C.-K. Sun, "Terahertz air-core microstructure fiber," Appl. Phys. Lett. **92**, 064105 (2008).
23. S. Atakaramians, S. Afshar Vahid, B. M. Fischer, D. Abbott, and T. M. Monro, "Loss mechanisms for T-ray microwires," in *Joint 32st International IEEE Conference on Infrared and Millimeter Waves and 15th International Conference on Terahertz Electronics*, pp. 811–812 (Cardiff, UK, 2007).
24. D. F. C. Zhao, M. Wu and S. Wen, "Field enhancement and power distribution characteristics of subwavelength-diameter terahertz hollow optical fiber," Opt. Commun. **281**, 1129–1133 (2008).
25. G. S. Wiederhecher, C. M. B. Corderio, F. Couny, F. Benabid, S. A. Maier, J. C. Knight, C. H. B. Crus, and H. l. Fragnito, "Field enhancement within an optical fibre with a subwavelength air core," Nat. Photonics **1**, 115–118 (2007).
26. T. M. Monro, "Beyond the diffraction limit," Nat. Photonics **1**, 89–90 (2007).
27. S.-Y. Wang, "Microstructured optical fiber with improved transmission efficiency and durability," United States Patent **US6418258B1** (2002).
28. S. Atakaramians, S. Afshar Vahid, B. M. Fischer, H. Ebendorff-Heidepriem, T. M. Monro, and D. Abbott, "Low loss terahertz transmission," in Proc. SPIE **6414**, 64140I (2006).
29. A. Zheltikov, "Gaussian-mode analysis of waveguide-enhanced Kerr-type nonlinearity of optical fibers and photonic wires," J. Opt. Soc. Am. B **22**, 1100–1104 (2005).
30. A. W. Snyder and J. D. Love, *Optical Waveguide Theory* (Kluwer academic publisher, London, 2000).
31. J. C. Baggett, T. M. Monro, K. Furusawa, V. Finazzi, and D. J. Richardson, "Understanding bending losses in holey optical fibers," Opt. Commun. **227**, 317–335 (2003).
32. H. Ebendorff-Heidepriem, and T. M. Monro, "Extrusion of complex preforms for microstructured optical fibers," Opt. Express **15**, 15086–15092 (2007).
33. S. Afshar V., and T. M. Monro, "Kerr nonlinearity in small core optical fibers and nanowires: a generalized model, and application to microstructured fibers," in *OECC/ACOFT*, (Sydney, Australia, 2008), accepted.
34. H.-W. Chen, Y.-T. Li, C.-L. Pan, J.-L. Kuo, J.-Y. Lu, L.-J. Chen, and C.-K. Sun, "Investigation on spectral loss characteristics of subwavelength terahertz fibers," Opt. Lett. **32**, 1017–1019 (2007).

1. Introduction

The terahertz (THz) or T-ray region of electromagnetic spectrum, located between millimeter wave and infrared frequencies, has attracted much interest over the last decade. The frequency range is loosely defined as 0.1-10 THz [1]. Terahertz spectroscopic techniques have many applications, as for example in detection of biological and chemical materials [2, 3]. Many of these preliminary proof-of-principle studies have been carried out in spectroscopy systems, where terahertz radiation propagates in free space. For biomedical applications, however, these systems have limitations such as large diffraction limited focal spot size leading to the need for inconveniently large biosamples [1], and the systems are quite large thus not easy to integrate with optical and infrared techniques. Terahertz waveguides provide a promising approach for overcoming these hurdles and potentially provide low-cost and robust THz integrated systems. However, efficient low-loss transmission of THz radiation within waveguides is still a challenge.

Waveguide solutions based on technologies from both electronics and photonics have been studied such as the hollow metallic circular waveguide [5], hollow metallic rectangu-

lar waveguide [6], sapphire fiber [7], plastic ribbon waveguide [8], air-filled parallel-plate waveguide [9, 10], plastic photonic crystal fiber [11], coaxial waveguide [12], metal wire waveguide [13, 14], parallel-plate photonic waveguide [15], metal sheet waveguide [16], sub-wavelength plastic fibers [17], the dielectric-filled parallel-plate waveguide [18], low-index discontinuity terahertz waveguides [19], and the metallic slit waveguide [20].

Metallic waveguide solutions based on bare metal wires, and dielectric fiber solutions based on sub-wavelength plastic fibers (described as THz microwires [21] in analogy with optical nanowires) and air-core microstructure fibers, with attenuation constants less than 0.03 cm^{-1} [13], 0.01 cm^{-1} [17], and 0.01 cm^{-1} [22] respectively, have the lowest loss reported in the literature. The guiding mechanism in sub-wavelength plastic fibers is based on the total internal refection, while in the air-core microstructure fiber is based on band gap effect. Low losses are achieved in bare metal wires and microwires, because almost all the field propagates in the medium surrounding the structure. This medium is usually air, which is transparent to THz. In other words, these structures act as rails for guiding THz radiation rather than as pipes that provide confinement. This, however, results in weak confinement of the guided field within the structure that makes the guided field susceptible to any small perturbation on the surface or vicinity of the structure, since a large portion of the guided power can be readily coupled into radiation modes. Furthermore, as a result of weak confinement, the guided modes within these structures suffer strong bend loss [19, 23]. To produce practical waveguide structures for THz, it is critical to find a means of improving the mode confinement while retaining the reduction in material loss that is associated with locating most of the guided field in air.

An approach to improve field confinement in the structure has been demonstrated by Nagel et al. [19]. They have shown that a low index discontinuity in dielectric waveguides (split rectangular and tube waveguides) has increased field in the low-index central region and reduced field in the air-clad surrounding region, resulting in increased confinement. Nagel et al. [19] demonstrated that a sub-wavelength air gap in a dielectric slab waveguide can trap 55% of the mode power in the vicinity of the gap between the two slabs, and a sub-wavelength hole in a fiber can trap 26% of the power in the sub-wavelength discontinuity. The former is difficult to handle because it needs another structure to keep the slabs together and the latter is not a promising low-loss waveguide structure for terahertz since a large portion of the power of the guiding mode is still propagating inside the material [24].

In this paper, we propose a novel class of fiber for THz, based on introducing sub-wavelength low index discontinuities within air-clad fibers. Instead of having one sub-wavelength air-hole in the core of the fiber [25, 26], we consider a pattern of sub-wavelength air-holes in the core, and show that this leads to a better confinement of the field to the structure while still allowing THz propagation in the sub-wavelength air-holes. In the optical regime, elongated void regions have previously been used to improve the transmission efficiency simply by reducing the material used within the core [27]. This paper considers a *porous fiber* core with sub-wavelength holes to enable localization and enhancement of the guided mode within the holes, and the use of such structures for improving the effective material loss and confinement. Here, we theoretically investigate the physics of THz propagation in porous fibers and examine the effective material loss and the confinement of THz propagation as a function of fiber porosity and diameter, in comparison with those of THz microwires (straight dielectric rods). We demonstrate that for similar loss values, our porous core fiber leads to better confinement than microwires.

2. Porous fiber

Porous fibers in this study are created by including a distribution of sub-wavelength air holes within the *core* of an air-clad fiber. A typical example is shown in Fig. 1(a). The distribution, shape, and size of the holes determine the porosity of the structure, which is defined as the

fraction of the air holes to core area. The structure shown in Fig. 1(a) has a triangular lattice of circular holes with radii of 20 μm, core radius of 200 μm, which results in a porosity of 37%. This sparse porosity value is only chosen for purposes of clarity for displaying the concept in Fig. 1. The arrangement of the holes within the core of porous fiber can be based on different varieties of lattice structures. We chose a triangular lattice because it leads to higher porosity when compared to a rectangular lattice of circular holes. Polymethyl methacrylate (PMMA) is considered as the host material for all of simulations here where we use the THz properties of PMMA (refractive index and attenuation constant as a function of frequency) [28] measured by THz time-domain spectroscopy (THz-TDS).

To find the propagation constant and field distributions for the porous fibers, we solve the full vectorial form of Maxwell's equations since, for the sub-wavelength scales considered here, a scalar approximation gives inaccurate results [29]. To solve Maxwell's equations for this geometry we use the Finite Element Modeling (FEM) technique instantiated in the commercial FEM package COMSOL 3.2. Considering the symmetry of the structure, we employ a quarter-plane of the fiber's cross-section and appropriate combination of perfect electric and magnetic conductor boundary conditions in order to determine the propagation constant and mode distribution. Different mesh densities are employed in different regions within the cross section in order to achieve convergence for the calculated parameters. The calculated propagation constant of the fiber is accurate to five significant figures and all other parameters presented in this paper are accurate to three significant figures. For calculating the THz microwire parameters, we use the solution of the vectorial Maxwell's equation in cylindrical coordinates for a circular cross-section step-index fiber with an infinite air cladding [28].

At any interface between two materials with no surface charge, since the normal components of the electric displacement field are continuous, there is a discontinuity in the electric-field strength; i.e., the electric-field enhances on the low refractive index side. The strength of the enhanced electric field depends on the square of the ratio of refractive indices and the electric field strength at the high index side. As a result, a higher enhanced electric field is formed at a low-index discontinuity interface, if it is introduced within a region of a waveguide structure where the electric field is originally stronger than the other regions. The enhanced electric field at the low index side of any discontinuity rapidly decays away from the interface discontinuity. However, if the dimension of the low index discontinuity is at the sub-wavelength scale, the decay of the evanescent field within the discontinuity is minimal. Thus a localized intensity enhancement can be achieved throughout the discontinuity region [25, 26].

The concept of field enhancement within low-index discontinuity (as explained above) is demonstrated in Fig. 1(b) which shows the normalized z-component of the Poynting vector ($S_z = \frac{1}{2}\vec{E} \times \vec{H} \cdot \hat{z}$) profile of the fundamental mode of the porous fiber along the arrow shown in Fig. 1(a). The refractive index profile along the same axis is also shown, demonstrating where the sub-wavelength air-holes are located. The refractive indices $n_1 = 1.6$ and $n_0 = 1$ refer to material (PMMA) and air refractive indices, respectively. The field is enhanced at the each air-material interface and stays localized in the sub-wavelength air-holes, where the refractive index is n_0. This phenomenon occurs for all the sub-wavelength air-holes in the structure as can be seen in Fig. 1(c). Since the enhancement coefficient at each interface is constant, n_1^2, the intensity of the localized field depends on the location of the sub-wavelength air-hole position. The closer the sub-wavelength air-hole to the center of the fiber, where the electric field intensity is stronger, the stronger the localized electric field intensity. Therefore the envelope of the intensified profile of the field has the same profile pattern of the air-clad fiber without sub-wavelength holes. For the chosen porous fiber dimensions, the power profile envelope has a Gaussian shape, Fig. 1(d). To find out the effect of these sub-wavelength air-holes on the fiber parameters, we evaluate the loss (effective material loss) and the confinement of THz propaga-

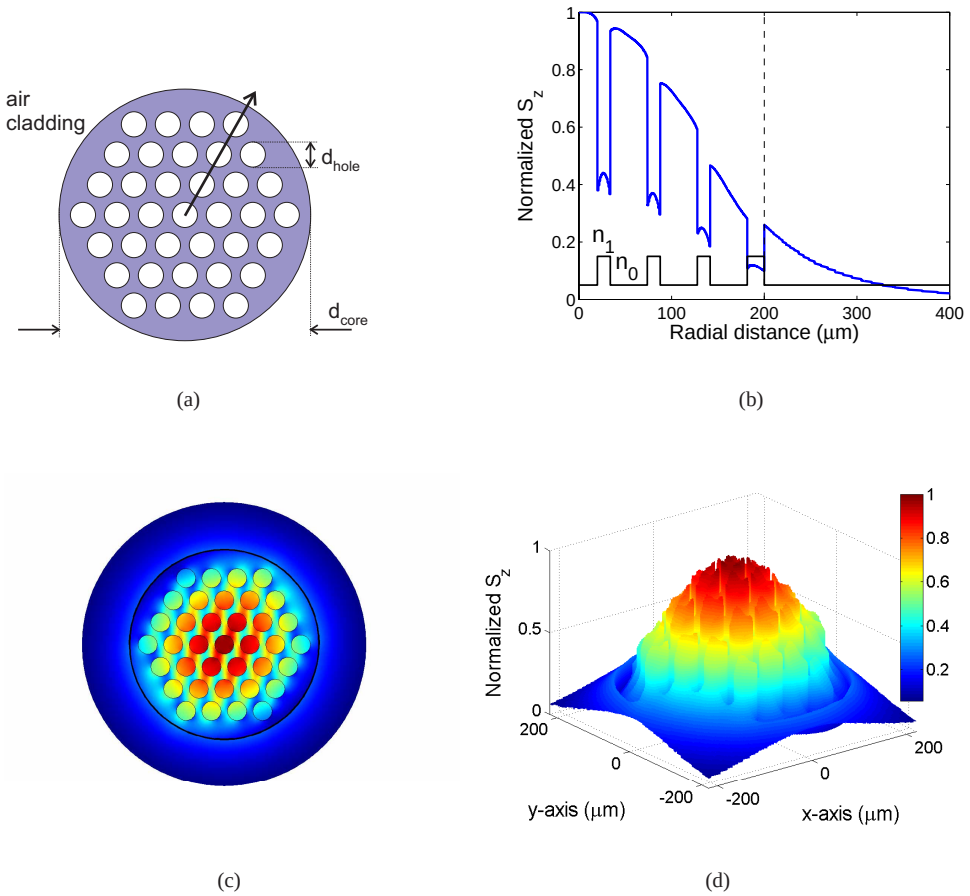

Fig. 1. (a)- Cross section and geometrical definitions of the triangular lattice porous fiber. (b) The normalized z-component of the Poynting vector, S_z, profile along the cross-section shown in (a), of the fundamental mode of a polymer porous fiber with core radius of $d_{\text{core}}/2 = 200$ μm, hole radii of $d_{\text{core}}/2 = 20$ μm and 37% porosity at $f = 0.5$ THz ($\lambda = 600$ μm). The dashed line represents the core to cladding interface and the lower solid line represents the refractive index profile. (c) 2D and (d) 3D view of the normalised S_z of the porous fiber.

tion in the following section.

3. Loss and confinement

In this section we calculate the optical parameters—i.e. power fraction, effective material loss and fraction of power lost as radiation in bend described below—of the porous fiber and compare them with those of a microwire. For convenience we consider three different regions within a porous fiber; sub-wavelength air-holes (region I), solid core material (region II) and the air cladding (region III). The fraction of the guided mode power (η) that is located within each

region can be defined as:

$$\eta_{\mathrm{x}} = \frac{P_{\mathrm{x}}}{P_{\mathrm{total}}} = \frac{\int_{\mathrm{A_x}} S_z dA}{\int_{\mathrm{A_\infty}} S_z dA}, \tag{1}$$

where, S_z is the z-component of the Poynting vector, the subscript $\mathrm{x} = \{\mathrm{I}, \mathrm{II}, \mathrm{III}\}$ represents each region, $dA = rdrd\phi$, and A_∞ and A_x are the infinite and region x cross-sections, respectively. Figure 2 shows the power fractions versus fiber diameter of three porous fibers with fixed porosities—61% (black lines), 70% (green lines) and 74% (blue lines)—at $f = 0.5$ THz ($\lambda = 600$ μm). At this frequency the optical parameters of the PMMA are $n = 1.6$ and $\alpha_{\mathrm{m}} = 4.2$ cm^{-1}. The solid, dashed and dotted lines demonstrate the power fraction in the regions I, II, and III, respectively. To maintain a fixed porosity, while the diameter changes for each structure, we keep the ratio of the air-holes to core diameter constant (0.1, 0.8 and 0.05 for 61%, 70% and 74% porosity respectively), i.e. all the dimensions of the fiber are scaled up. It should be noted that for every porosity value there is an upper limit for the core diameter, where the power fraction lines stop in Fig. 2, beyond which the material between the sub-wavelength air-holes begins to act as an array of independent sub-wavelength fibers. The core diameter at which this occurs depends on the porosity of the fiber, i.e., for higher porosity values the limit is larger, indicating that the structure stays in the porous fiber regime for a wider range of diameters. Therefore, no data is shown beyond this limit in the following figures. For comparison, the power fractions in the air-clad (dashed line) and solid core (dotted line) of a THz microwire have also been evaluated and sketched in red in Fig. 2.

For large fiber diameters ($d_{\mathrm{core}} \geq \lambda$), most of the guided power of the THz microwire is located in the solid core, while the power fraction residing in the sub-wavelength air-hole region [solid black, green, and blue lines in Fig. 2] of the porous fiber is dominant. The diameter increase in the porous fiber does not have a significant effect on the power fraction in the core material, η_{II}, [dotted blue, green, and black lines in Fig. 2] while there is a considerable change in η_{I} and η_{III}. This means that by increasing the fiber diameter most of the power in the air-clad region is transferred to the sub-wavelength air-holes. This is an advantage over the THz microwire, in which increasing the diameter increases the power fraction in the solid-core of the fiber, and it results lower material loss of THz propagation in the porous fiber in comparison to that of the THz microwire. This is more evident in Fig. 3 and is discussed later on.

Unsurprisingly, for sub-wavelength diameters ($d_{\mathrm{core}} << \lambda$), porous fibers and THz microwire have a similar behavior, i.e., the power fractions in the core of both waveguides (η_{I} and η_{II} for porous fibers) decrease as the diameter decreases and most of the power is transferred to the air-clad region. However, the influence of the small percentage of the power residing in the sub-wavelength air-holes of the porous fiber (η_{I}), is noticeable in the loss values.

There are two major loss mechanisms to be considered for these fiber structures, effective material loss and bend loss. Effective material loss is a measure of the loss that a guided mode with a certain mode field distribution experiences when it propagates along a fiber with an inhomogeneous loss coefficient profile in transverse direction. The effective material loss, α_{eff}, of a guided mode is defined as [30]:

$$\alpha_{\mathrm{eff}} = \frac{(\varepsilon_0/\mu_0)^{1/2} \int_{\mathrm{A_\infty}} n(r)\alpha_{\mathrm{m}}(r)\,|E|^2\, dA}{\left|\int_{\mathrm{A_\infty}} S_z dA\right|}, \tag{2}$$

where, $\alpha_{\mathrm{m}}(r)$ is the material absorption loss, $n(r)$ is the refractive index, ε_0 and μ_0 are the permittivity and permeability of free space, respectively. Since air is a transparent medium for THz (negligible absorption coefficient $\alpha_{\mathrm{m}} = 0$), the integration in the numerator of the Eq. 2 is

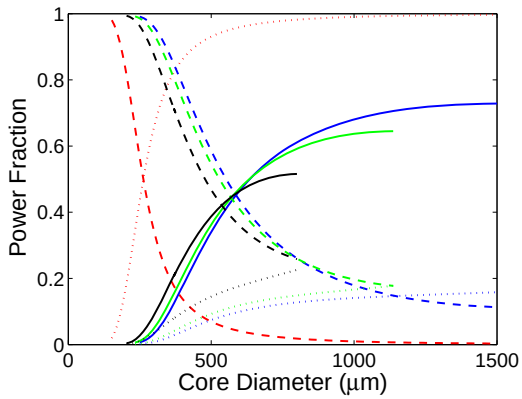

Fig. 2. Power fraction in the air holes (solid lines), core material (dotted lines) and air-clad (dashed lines) versus fiber diameter of a THz microwire (red lines) and porous fibers of 61% (black lines), 70% (green lines) and 74% (blue lines) porosity at $f = 0.5$ THz ($\lambda = 600$ μm).

performed only over the solid core area. Figure 3 shows the effective material loss of porous fibers and a THz microwire at $f = 0.5$ THz ($\lambda = 600$ μm). Owing to porosity of the core, it is evident in Fig. 3 that for similar diameters the effective material loss of these fibers is less than that of the THz microwire. Moreover for porous fibers the effective material loss decreases as the porosity increases, since less material resides in the core. For sub-wavelength diameters ($d_{\text{core}} << \lambda$), the effective material loss declines to the same order for all the structures with different descending slopes. For porous fibers the loss starts declining from a lower loss value over a larger diameter range, indicating that the effective material loss of porous fiber is less sensitive to diameter variation when compared to that of THz microwires. This is more evident in Fig. 5 and is discussed later on.

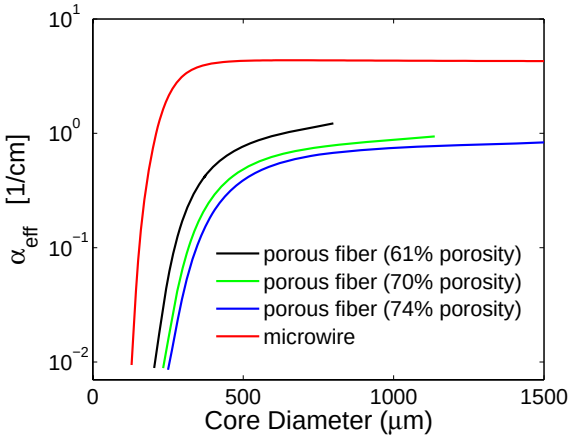

Fig. 3. Effective material loss versus fiber diameter of a THz microwire (red line) and porous fibers of 61% (black line), 70% (green line) and 74% (blue line) porosity at $f = 0.5$ THz ($\lambda = 600$ μm).

Pure bend loss is defined as the continual loss of radiation that occurs along any curved

section of fiber and is related to the inability of the tail of the mode to successfully navigate the bend. For a mode propagating along a curved trajectory, the local velocity along the phase fronts of the mode must decrease on the inside of the bend and increase on the outside of the bend in order to maintain a constant angular velocity across the mode. If we consider the guided mode propagation in the z direction around a bend in the x-plane, at some distance towards the outer tail of the mode ($x = x_r$) the required phase velocity will exceed the local speed of light. This distance from the center of the fiber is given by [31]:

$$x_r = \left(\frac{\beta_b}{\beta_{FSM}} - 1 \right) R_o, \tag{3}$$

where R_o is the bend radius and β_b and β_{FSM} are the propagation constants of the mode of the bent fiber and the fundamental space-filling mode of the cladding, respectively. For the air-clad fibers discussed in this paper $\beta_{FSM} = k$, where $k = 2\pi/\lambda$. Since the power beyond x_r is lost as radiation, the structure with more power in the tail beyond this point experiences higher bend loss. Figure 4 shows the fraction of power beyond x_r, η_{rad}, for a porous fiber with a 74% porosity (solid lines) and a microwire (dashed lines) as a function of effective material loss for two bend radii, 20 cm and 50 cm. It is evident that if a porous fiber and microwire with an identical effective loss value experience the same bend radius, the fraction of power lost as radiation for porous fiber is lower than that of microwire. This is due to the power fraction in the sub-wavelength air-holes of the porous fiber since the power in these holes is still in the air, but confined to the structure. It should be noted that as soon as x_r gets smaller than the core radius of porous fiber, the power radiated beyond x_r of the porous fiber approaches to that of the microwire. This indicates that for similar effective material loss values the mode is more confined to the porous fiber compared to microwire. For evaluating the bend loss values, of the fibres, more detailed calculation is required.

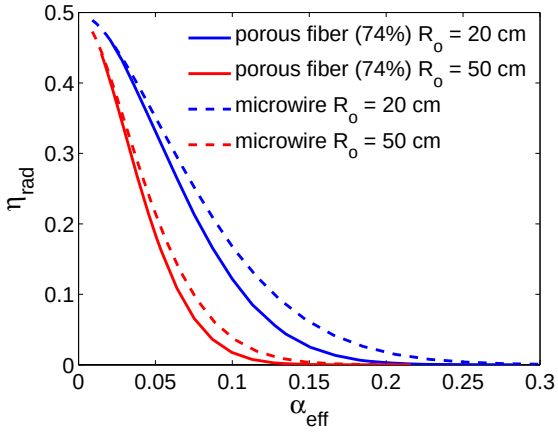

Fig. 4. Fraction of power beyond x_r lost as radiation in bends, η_{rad}, versus effective material loss of a THz microwire (dashed line) and porous fibers of 74% porosity (solid line) for two bend radii (20 cm and 50 cm) at $f = 0.5$ THz ($\lambda = 600$ μm).

In order to compare the frequency dependence of the effective material loss of porous fibers and microwires, we evaluate the effective material loss variation versus frequency for a porous fiber with a 74% porosity and a THz microwire versus frequency for three different diameters, Fig. 5. The measured attenuation constant of bulk PMMA [28], determined via THz-TDS, is used for calculation of the effective material loss. As shown in Fig. 5, a porous fiber of diameter

500 μm (black solid line) and microwire of diameter 250 μm (black dashed line) have the same order of effective material loss at $f = 0.2$ THz ($\alpha_{\text{eff}} < 0.01$ cm^{-1}) and by increasing the frequency the loss in both of them increases. However, the increase in α_{eff} the of porous fiber is less pronounced when compared to that of the microwire. For frequencies larger than 0.4 THz the effective material loss of the porous fiber is three orders of magnitude lower than that of the microwire. This implies that the porous fiber causes less distortion (due to the loss) of broad-spectrum pulses when compared to that of the THz microwire.

Additionally, Fig. 5 indicates that the porous fiber is less sensitive to diameter changes compared to the microwire. A 20% increase in the core diameter of the fibers, that results in 500 μm and 250 μm diameter of porous fiber and microwire respectively shown in Fig. 5, changes the lower limit of effective material loss of the microwire an order of magnitude and the porous fiber less than a third of an order of magnitude. This is due to the fact that in porous fibers there is less material residing in the core compared to microwires. This difference is more noticable for 60% diameter change, resulting in a 800 μm diameter of porous fiber and 400 μm diameter of microwire, as shown in Fig. 5.

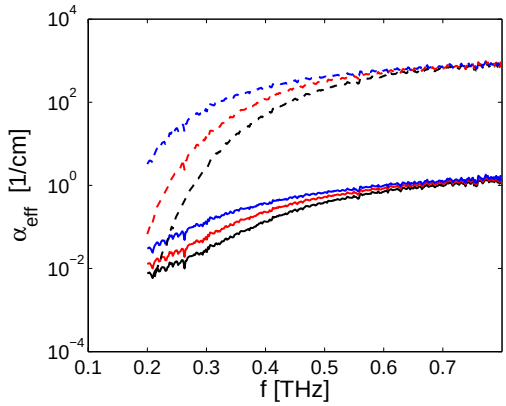

Fig. 5. Effective material loss versus frequency of a porous fiber with a 74% porosity (solid lines) with 500 μm (black), 600 μm (red) and 800 μm (blue) diameters and a sub-wavelength fiber (dashed lines) with 250 μm (black), 300 μm (red) and 400 μm (blue) diameters. For comparison the geometrical area of the core is also depicted with a dotted-dashed black line.

4. Discussion and conclusion

Compared to a microwire, a porous fiber offers the same order of loss with less susceptibility to the bend loss and environment external to the fiber, thus reducing the practical handling issues. Although both are air-clad fiber structures, due to the power residing in the sub-wavelength air-holes of porous fiber, any disturbance in the air-clad region of the porous fiber leads to significantly lower distortion of the field distribution. As a result of strong localized field in the sub-wavelength air-holes, the porous fiber has potential application in THz gas and liquid spectroscopy. However, the manufacturing process for porous fiber is more challenging than the equivalent microwire, especially for higher porosity values. Having said that, the dimension of the holes (10-30 microns) and the core diameter (300-1000 microns) are larger than those of the microstructured optical fibers (MOFs) manufactured for the visible and near infrared spectrum. Recently, MOFs made up of soft glass and polymer with a large air fraction and holes of 1-2 microns diameter have been successfully fabricated [32], indicating that the fabrication process

of THz porous fiber will be easier to implement than the optical counterpart.

A practical consideration for porous fibers is the coupling efficiency. Due to sub-wavelength features within the structure, the commonly used coupling coefficient [17], calculated based on weakly guiding approximation, fails to give the accurate results. For these types of fibers the *z* component of the propagating mode of the fiber becomes important, as has recently been pointed out [33]. Therefore a full vectorial version of coupling efficiency considering the radiation modes and scattering at the tip of the porous fiber should be considered. Moreover the diameter-variation induced radiation, which is a limiting mechanisms for the lowest guidable frequency in sub-wavelength fiber [34], possibly due to both outer surface and sub-wavelength hole surfaces, should be considered. It is expected that the radiation due to outer surface variation to be less pronounced in porous fibers, in comparison with that of microwires, due to their larger core diameter and lower power fraction in the air-clad for an identical effective material loss. For example in Fig. 3, at $\alpha_{\text{eff}} = 0.1$ cm^{-1} porous fiber and microwire have the diameters of 345 and 153 μm and corresponding power fraction, η_{III}, of 89% and 98%, respectively. It is also worth mnetioning that the typical diameter variations in the fabrication process is the order of ± 1 μm, which results in less relative diameter variation for proous fiber (0.3%) compared to that of the microwire (0.7%).

In conclusion, we have proposed a new fiber structure for the THz regime, a porous core fiber, based on a sub-wavelength low index discontinuity at the material-air interface. We have considered a triangular pattern of circular holes within the core of the an air-clad fiber and have shown that this leads to an improved confinement of the field to the structure while still allowing THz propagation in the sub-wavelength holes. We have investigated the loss (effective material loss) and the confinement of THz propagation as a function of fiber porosity and diameter and compared them with those of THz microwires. We demonstrate that for similar loss values, the porous fiber leads to better confinement than microwires. It has also been shown that, the loss of a porous fiber is a much flatter function of frequency and less sensitive to diameter variations. Thus, for applications with broadband pulses, porous fiber has reduced loss distortion compared to the THz microwire.

Acknowledgment This research was supported under the Australian Research Council's (ARC) *Discovery Projects* funding scheme (project numbers DP0556112 and DP0880436). Useful discussion with Barry Luther-Davies of the Australian National University (ANU) on the microwire aspect is gratefully acknowledged.